Available online at www.sciencedirect.com
ScienceDirect
Journal of Nuclear Materials 363–365 (2007) 41–51
journal of nuclear materials
www.elsevier.com/locate/jnucmat

Understanding the SOL flow in L-mode plasma on divertor tokamaks, and its influence on the plasma transport

Nobuyuki Asakura, ITPA SOL and Divertor Topical Group

Japan Atomic Energy Agency, Mukouyama 801-1, Naka, Ibaraki-ken 311-0193, Japan

Abstract

Significant progress has been made in understanding the driving mechanisms in SOL mass transport along the magnetic field lines (SOL flow). SOL flow measurements by Mach probes and impurity plume have been performed in L-mode plasma at various poloidal locations in divertor tokamaks. All results showed common SOL flow patterns: subsonic flow with parallel Mach number ($M_{\|}$) of 0.2–1 was generated from the Low-Field-Side (LFS) SOL to the High-Field-Side (HFS) divertor for the ion ∇B drift towards the divertor. The SOL flow pattern was formed mainly by LFS-enhanced asymmetry in diffusion and by classical drifts. In addition, divertor detachment and/or intense puffing-and-pump enhanced the HFS SOL flow. Most codes have incorporated drift effects, and asymmetric diffusion was modelled to simulate the fast SOL flow. Influences of the fast SOL flow on the impurity flow in the SOL, shielding from core plasma, and deposition profile, were directly observed in experiments.

PACS: 52.25.−b

Keywords: Plasma flow; Particle drift; Mach probes; Impurity transport; Divertor modelling

1. Introduction

SOL mass transport along the magnetic field lines (SOL flow) is of direct relevance to particle control with divertor pumping and impurity screening properties. At the same time, fast SOL flow around the main plasma (main SOL) plays an important role in long-range transport of the first wall and divertor materials [1]. In the past years, significant progress has been made in understanding the flow pattern and the driving mechanisms partly due to development of flow measurements at important poloidal locations, and partly due to improvement of the modelling and simulation codes. In particular, subsonic level of the SOL flow was determined by both Mach probe and spectroscopy measurements, and the fast SOL flow can be simulated with introducing classical drifts and in–out asymmetry in diffusion. This paper reviews recent progress in the measurements and the driving mechanisms.

The SOL flow profile changes along the field lines. The three-dimensional flow pattern is presented in Section 2. Understanding of the flow mechanisms from an experimental approach, i.e.

E-mail address: asakura.nobuyuki@jaea.go.jp

0022-3115/$ - see front matter © 2006 Published by Elsevier B.V.
doi:10.1016/j.jnucmat.2006.12.029

using Mach probe measurements, is summarized in Section 3. Results of modelling and simulations with classical drifts and asymmetrical diffusion are summarized in Section 4. Recent results on impurity plume measurement, carbon deposition, and impurity shielding during intense puff-and-pump are discussed in Section 5, showing influences of the SOL flow on impurity transport. Finally, conclusions are described in Section 6.

2. SOL flow measurements

SOL flow measurements by Mach probes have been performed at different poloidal locations in many tokamaks such as JT-60U [2,3], JET [4,5], AlcatorC-MOD (C-MOD) [6,7], TCV [8], DIII-D [9], ASDEX-Upgrade (AUG) [10,11], and ToreSupra [12]. Corresponding poloidal locations of the Mach probe measurements are illustrated in Fig. 1(a). Fig. 2 shows the radial profiles of Mach number of the SOL flow ($M_{\|}$) in L-mode plasmas on JT-60U, JET and C-MOD. Three cases are lower single-null divertor configuration with the ion $\mathbf{B}\times\nabla B$ drift direction towards the divertor, and the main plasma density ($\bar{n}_e$) normalized by the 'Greenwald density' (n^{GW}) is relatively low ($\bar{n}_e/n^{GW} = 0.4$–0.45). $M_{\|}$ is deduced from the ratio of the ion saturation currents at the electron- and ion-sides (j_s^e and j_s^i), using Hutchinson's formula [13]: $M_{\|} = \alpha \ln[j_s^e/j_s^i]$, where $\alpha = 0.3$–0.4. In the simple SOL model, the SOL flow is generated towards the divertor due to parallel gradients of plasma pressure. However, at LFS of the main SOL, upward SOL flow (opposite to what one would expect from the simple picture, i.e. 'flow reversal') is generally observed in many tokamaks (JT-60U, C-MOD, TCV, AUG). At the same time, $M_{\|}$ becomes subsonic level ($M_{\|} = 0.3$–0.4) near the separatrix. At the plasma top (JET), fast SOL flow is found continuously towards the HFS SOL, and radial location of the maximum $M_{\|}$ extends to the outer flux surfaces (far SOL). Fast SOL flow with $M_{\|} = 0.3$–0.5 at the plasma top is observed also in the bottom limiter configuration (ToreSupra). Measurements in the HFS SOL (JT-60U, C-MOD) show the maximum $M_{\|}$ is increased to sonic-level (from 0.5 to larger than 1), whereas measurements of $M_{\|}$ in the narrow region near the separatrix show no (C-MOD) or small flow towards the plasma top ($M_{\|} \sim -0.15$ in JT-60U). It is noted that similar SOL flow pattern, i.e. parallel flow towards the LFS midplane to the HFS divertor with comparable

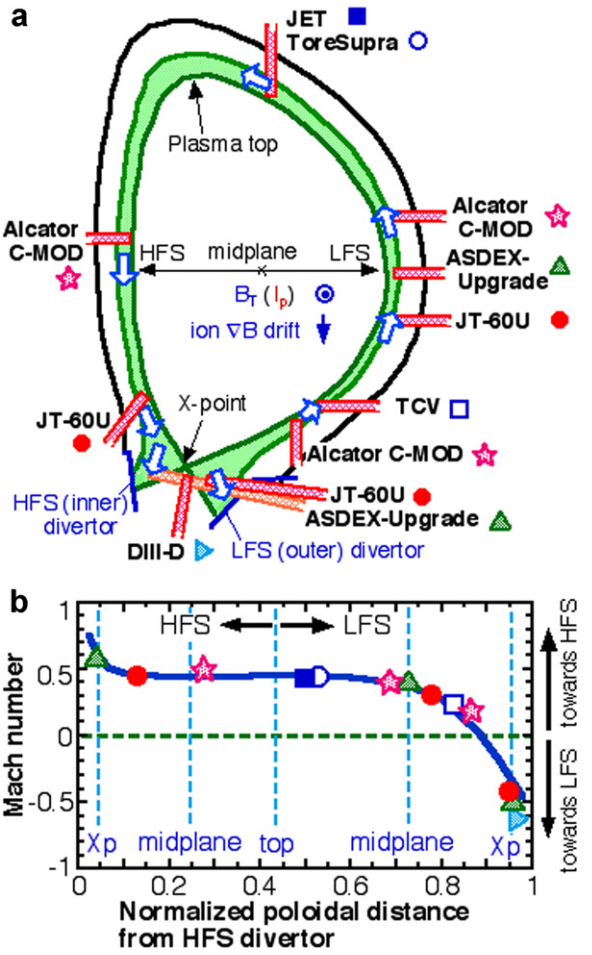

Fig. 1. Illustration of poloidal locations of the Mach probe measurements for the lower single-null divertor operation in tokamaks such as JT-60U, JET, Alcator C-MOD, TCV DIII-D, ASDEX-Upgrade, and ToreSupra (lower limiter). (b) Typical values of $M_{\|}$ near the separatrix ($r^{mid} < 2$ cm) in medium $\bar{n}_e/n^{GW}$ range (0.4–0.5) for the ion $\mathbf{B}\times\nabla B$ drift direction towards the divertor. Symbols correspond to tokamaks shown above.

$M_{\|}$ in L-mode, was observed between ELMs in H-mode plasma of JT-60U [14], AUG [11] and JET [5]. Since there is limited number of database for the H-mode plasma, SOL flow in the L-mode diverted tokamak plasmas is reviewed in this paper.

All results are consistent with a fact that subsonic SOL flow is produced from LFS SOL to the HFS divertor for the ion $\mathbf{B}\times\nabla B$ drift direction towards the divertor, independent of the plasma shape and divertor geometry. On the other hand, in the LFS divertor, the SOL flow towards the divertor was observed in JT-60U [2], DIII-D [9] and AUG [10]. Typical $M_{\|}$ near separatrix ($r^{mid} < 2$ cm) for medium $\bar{n}_e/n^{GW}$ range (0.4–0.5) are plotted in

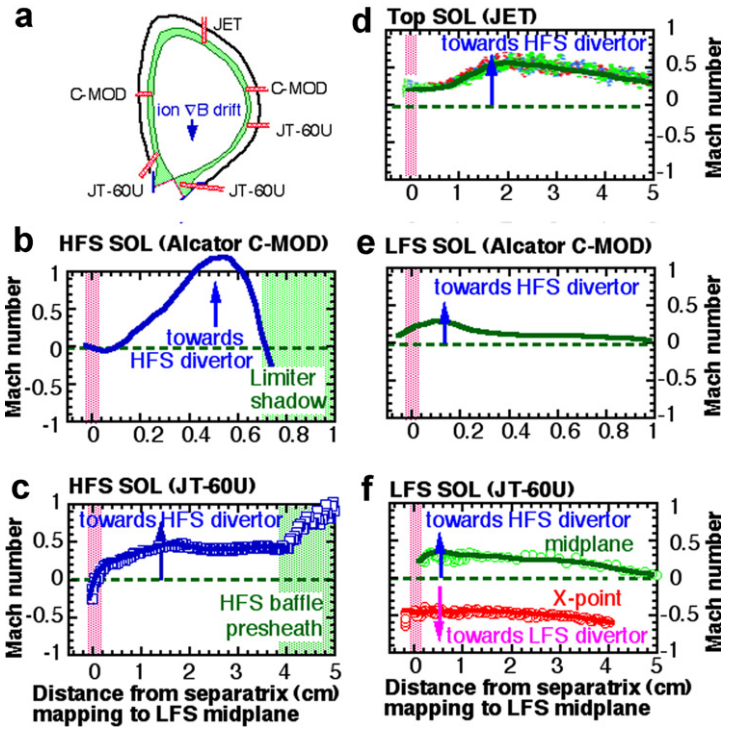

Fig. 2. SOL flow profiles measured with Mach probes (a) at the different poloidal locations in JT-60U, JET and C-MOD for the ion $\mathbf{B}\times\nabla B$ drift direction towards the divertor: (b) at HFS midplane [7], (c) above HFS baffle [3], (d) at plasma top [5], (e) above LFS midplane [7], (f) below LFS midplane and divertor null-point [2].

Fig. 1(b), suggesting that the 'stagnation point' is between the LFS midplane and the LFS SOL near the X-point.

3. Driving mechanisms of the SOL flow

The major mechanisms producing SOL flow in tokamaks are explained from the experimental point of view. Fig. 3 shows $M_{\|}$ profiles at the LFS midplane (C-MOD) and at the plasma top (JET) as $\bar{n}_e$ is increased for the ion $\mathbf{B}\times\nabla B$ drift direction *towards* and *away from* the divertor (*normal/forward* and *reversed* B_t, respectively). Results at the LFS midplane (C-MOD) show two general characteristics consistent with measurements in other tokamaks (JT-60U, TCV). One is that the direction of the SOL flow changes with B_t reversal (i.e. the SOL flow direction in poloidal projection at the LFS midplane is against the ion $\mathbf{B}\times\nabla B$ drift direction). Another is that the absolute value of $M_{\|}$ is decreased from 0.4 to 0.1 with increasing $\bar{n}_e$. On the other hand, at the plasma top, $M_{\|}$ is small in reversed B_t, and the direction towards the LFS changes to slightly towards the HFS SOL at higher $\bar{n}_e$. This suggests that B_t-independent component of the SOL flow ($\langle M_{\|}\rangle = 0.2$–$0.3$) is produced towards the HFS SOL [4], and that B_t-dependent component ($\Delta M_{\|}$) is comparable to $\langle M_{\|}\rangle$ (i.e. $\Delta M_{\|} = 0.2$–0.3). As a result, a combination of driving mechanisms such as one affected by the plasma drift and another independent of the B_t direction, forms the complicated SOL flow pattern. Classical drifts and edge rotation are discussed as candidates for the B_t-dependent flow in Sections 3.1 and 3.4, respectively. In–out asymmetry in edge diffusion and divertor detachment are investigated as candidates for the B_t-independent flow in Section 3.2 and 3.3, respectively.

3.1. Drift effects in tokamak

The classical drifts such as $\mathbf{E}\times\mathbf{B}$ and $\mathbf{B}\times\nabla B$ (and diamagnetic, $\nabla p\times B$, for fluid model) play an important role in perpendicular and parallel transports in toroidal geometry [15]. In the SOL, parallel flow, i.e. ion Pfirsch-Schlüter (PS) flow, can be produced due to in–out asymmetry of $E_r\times B$ and $\nabla p_i\times B$ drifts in the flux surfaces for the fluid model

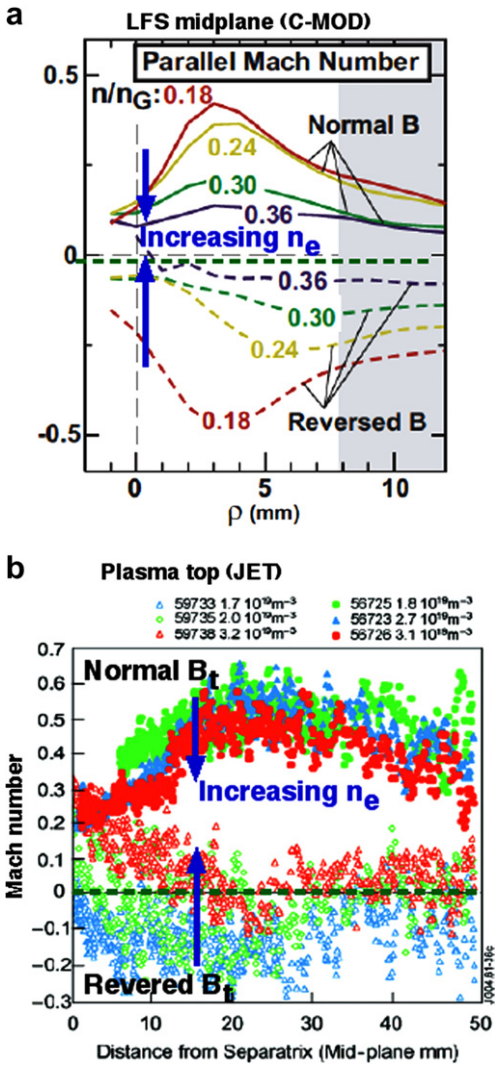

Fig. 3. Radial SOL flow profiles (a) at LFS midplane in C-MOD [7], and (b) at plasma top in JET [5], in density scan for normal and reversed B_t.

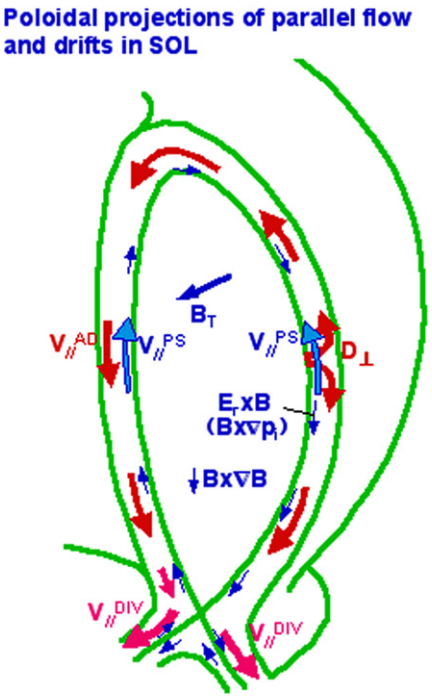

Fig. 4. Poloidal projections of parallel SOL flow components, i.e. ion Pfirsch-Schlüter flow ($V_{\parallel}^{PS}$), driven by in–out asymmetric diffusion ($V_{\parallel}^{AD}$) and plasma sink in divertor ($V_{\parallel}^{DIV}$), are illustrated by thick arrows. Projection of drifts in main SOL, i.e. $E_r \times B$, $\nabla p_i \times B$ and ion $\mathbf{B} \times \nabla B$ drifts, for normal B_t case are also shown by thin arrows.

[16,17]. Poloidal projections of the ion PS flow, and $E_r \times B$, $\nabla p_i \times B$ and ion $\mathbf{B} \times \nabla B$ drifts are illustrated in Fig. 4. The PS flow has the flow direction against the ion $\mathbf{B} \times \nabla B$ drift, and the theoretical formula in confined plasma, $V_{\parallel}^{PS} = 2q_s V_{\perp} \cos\theta$ (q_s is the safety factor, θ is poloidal angle, $V_{\perp} = [E_r - \nabla p_i/en_i]/B$ where $E_r \times B$ and $-\nabla p_i \times B$ are basically the same direction in SOL), has a maximum at the midplane. Simple evaluation of $V_{\parallel}^{PS}$ from measured T_i, T_e and V_f profiles was done at the LHS midplane for normal and reversed B_t cases in JT-60U [18] and TCV [8]. Mach numbers ($V_{\parallel}^{PS}/C_s$, C_s is the plasma sound velocity) and the reduction with increasing $\bar{n}_e$, due to reduction in E_r and ∇p_i at high $\bar{n}_e$,were consistent with Mach probe measurements. Thus, the general characteristics of the B_t-dependent flow ($\Delta M_{\parallel}$) at the LFS midplane can be explained by the PS flow, but its influence on $\Delta M_{\parallel}$ in the open field line may be smaller than the simple formula of $V_{\parallel}^{PS}$ and the diamagnetic contribution to $V_{\perp}$ is questionable in the SOL.

The analysis in terms of PS flow can be applicable to measurements at the HFS SOL of JT-60U and C-MOD. Fig. 5 shows $M_{\parallel}$ profiles at low and high $\bar{n}_e$ for normal and reversed B_t cases in JT-60U. At least, $\Delta M_{\parallel}$ near the separatrix ($M_{\parallel} = -0.2$ and $+0.2$ for normal and reversed B_t, respectively) can be explained by the PS flow. On the other hand, at the far SOL, fast SOL flow towards the HFS divertor is generated independent of the B_t direction, and their profiles can be described by $|\Delta M_{\parallel}| = 0.1$–$0.3$ at low $\bar{n}_e$ and it decreases at high $\bar{n}_e$, provided that $\langle M_{\parallel} \rangle$ is increased from 0 to the sonic speed level (0.8) with r^{mid}. Value of $\Delta M_{\parallel} \sim 0.3$ in the far SOL is larger than that the PS flow expected from the small E_r and $-\nabla p_i$, while the $\Delta M_{\parallel}$ direction is against the ion $\mathbf{B} \times \nabla B$ drift.

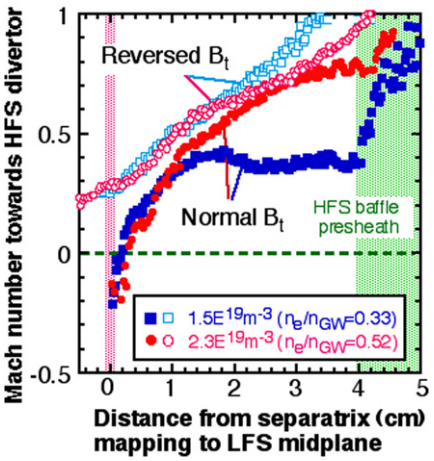

Fig. 5. HFS SOL flow profiles in density scan (circles and squares are attached and detached divertors, respectively) for normal and reversed B_t cases in JT-60U [3].

The drift effects on $M_{\|}(|\Delta M_{\|}| < 0.3)$ appear even at the plasma top (JET) and outer flux surfaces in the HFS SOL (JT-60U, C-MOD), where $\Delta M_{\|}$ is not expected from the simple formula of the PS flow.

3.2. Plasma pressure enhancement at LFS

In order to understand the driving mechanism of B_t-independent flow ($\langle M_{\|}\rangle$) towards the HFS divertor, a specific experiment was preformed in C-MOD ohmic L-mode plasma [7]. SOL plasma profiles at the HFS and LFS midplanes were measured in three divertor geometries: lower single null (LSN), upper single null (USN) and double null (DN) divertors as shown in Fig. 6, where the ion $\mathbf{B}\times\nabla B$ drift direction was downward. Here, the positive direction of the SOL flow is defined as the ion drift direction (i.e. CCW in poloidal cross-section). The USN divertor experiment corresponds to the reversed B_t case as discussed in Section 3.1. Profiles of electron pressure ($p_e = n_e T_e$) at the HFS and LFS midplanes are comparable for the LSN and USN cases. Fast SOL flow towards the HFS divertor is produced similarly for the two cases, except that $|M_{\|}| \sim 0.5$ near the separatrix for USN is much larger than $M_{\|} \sim 0$ for LSN. A unique result is obtained in the DN divertor as shown in Fig. 6(b). p_e becomes small at HFS midplane compared to that at LFS. At the same time, $|M_{\|}|$ is decreased to zero at the outer flux surfaces. In the connected SOL for the single-null divertors, the dominant particle transport in the HFS SOL appears to be the parallel flow from the LFS rather than the transverse transport, i.e. large part of the HFS SOL plasma is transported from the LFS SOL.

Plasma pressure balance between the HFS and LFS SOLs is investigated for the LSN and USN divertors as shown in Fig. 7. Generally, the static pressure component ($n_e T_e + n_i T_i$) plus the dynamic pressure component ($m_i[M_{\|}C_s]^2$) should be balanced along the field line, assuming no pressure/momentum source and loss in SOL. Provided that $T_i \sim T_e$ in the high density SOL ($n_e^{sep} \sim 1\times 10^{20}\ \mathrm{m}^{-3}$) of C-MOD, experiments show that the static pressure at the LFS is larger than that at the HFS, and that the SOL flow at the HFS is enhanced up to the subsonic level in order to balance the total pressure. Here, the increase in the LFS static pressure may

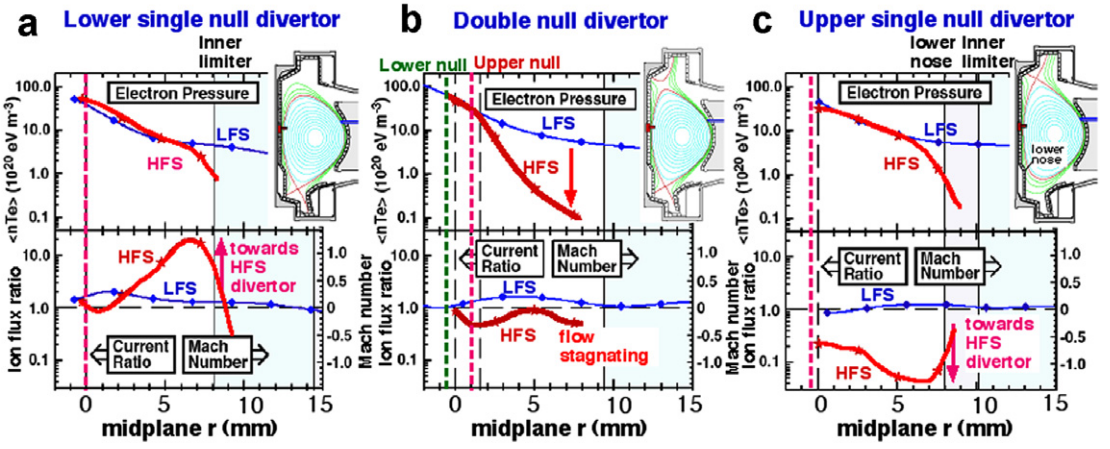

Fig. 6. Magnetic equilibrium (a) for lower single-null discharge and corresponding profiles of electron pressure and Mach number in the HFS and LFS midplanes of C-MOD. The same (b) for double null and (c) for upper-single null discharges [7].

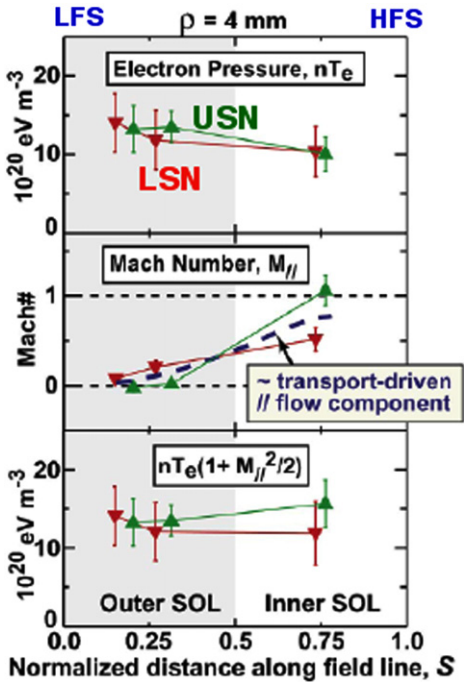

Fig. 7. Probe data, (a) electron pressure, (b) Mach number, and (c) total plasma pressure, mapped onto a flux tube coordinate system in C-MOD. $S = 0$ and 1 correspond to the LFS and HFS divertor throats in SOL. Upper and lower triangles correspond to normal and reversed B_t cases. Broken line in (b) presents B_t-independent component in the parallel SOL flow [20].

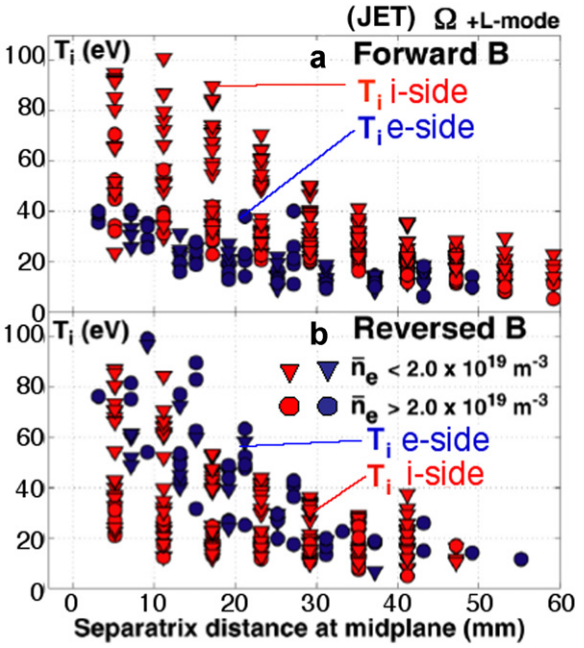

Fig. 8. Radial T_i profiles, ordered by density, on each side of the bi-directional RFA probe for (a) forward and (b) reversed B_t discharges in JET. For forward B_t case, i- and e-side RFAs face the SPL plasma respectively towards the LFS and HFS. For reversed B_t case, i- and e-sides change to HFS and LFS SOL. The data are obtained mostly during the ohmic phase of each pulse [19].

be caused by enhanced cross-field diffusion near or below the midplane for the ion $\mathbf{B}\times\nabla B$ drift direction towards the divertor. Models of in–out asymmetry in cross-field diffusion were recently developed, and influences of both drifts and the asymmetric diffusion are summarized in Section 4.

In addition to the in–out asymmetry, the precise poloidal location where large mass and energy fluxes are exhausted from the main plasma can be influenced by the ion $\mathbf{B}\times\nabla B$ drift. A Mach probe type of Retarding Field Analyzer (RFA) can measure both T_i and ion fluxes at electron- and ion-sides in the plasma top of JET [19] for the normal and reversed B_t cases, as shown in Fig. 8. T_i ratio is found to exhibit a similar behavior as that of the ion flux, shown in Fig. 3(b): T_i measured at the ion side is larger than T_i at the electron side for the normal B_t, whereas both T_i measurements are comparable for reversed B_t. Assuming that poloidal location of large energy outflux is shifted to downward and upward in LFS SOL for the normal and reversed B_t cases, respectively, the result would be explained. Investigation of the up–down asymmetry as well as the in–out asymmetry in the radial transport is required to understand B_t-dependent flows at the plasma top.

3.3. Influence of divertor detachment

Detachment of the divertor plasma causes momentum loss and thus modifies the pressure balance. Fig. 9 shows the change in $M_{||}$ profile above the HFS baffle with increasing n_e in JT-60U [3]. When the plasma detachment occurs at the HFS divertor, the $M_{||}$ profile changes: $M_{||}$ at far SOL is enhanced and finally reaches sonic-level during X-point MARFE at $\bar{n}_e/n^{GW} = 0.85$. Here, T_e values near the HFS SOL separatrix (T_e^{sep}) and at the far SOL (T_e^{far} at $r^{mid} \sim 3$ cm) decrease from 90 to 45 eV, and from 27 to 20 eV, respectively. Thus, reduction in C_s at the far SOL is small. As a result, large enhancement of the SOL flow (particularly the B_t-independent flow) up to sonic-level may be caused by detachment at the HFS divertor, in addition to increasing the plasma pressure at LFS SOL. In C-MOD, a sonic-level of $M_{||}$ is generally observed even at the HFS midplane as shown in

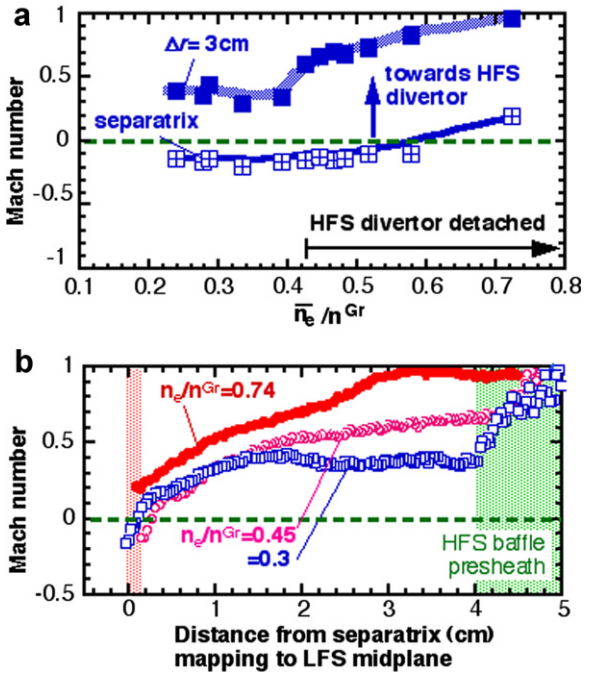

Fig. 9. (a) Mach number in the HFS SOL in JT-60U: near and far SOL ($\Delta r = 3$ cm mapping to LFS midplane) in density scan. (b) Mach number profiles at $n_e/n^{GW} = 0.3$ (attached divertor), 0.45 (HFS divertor detachment) and 0.74 (X-point MARFE).

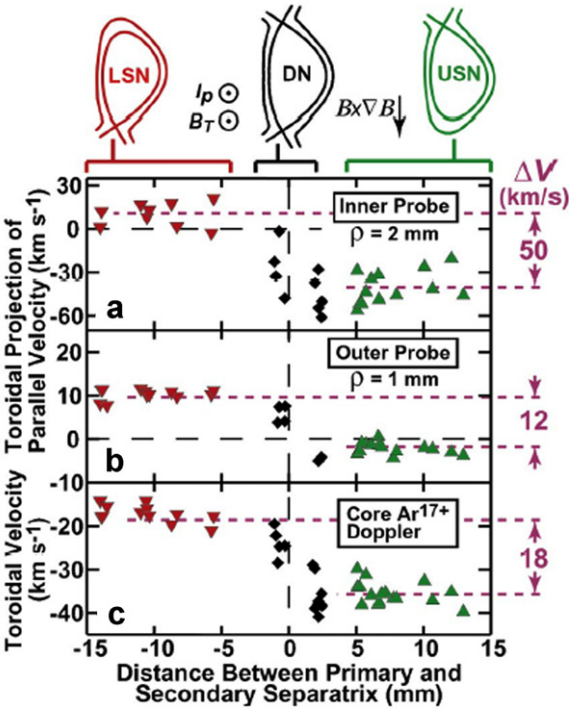

Fig. 10. Toroidal components of the parallel SOL flow at (a) HFS and (b) LFS midplanes, and (c) toroidal flow velocities in C-MOD as a function of the magnetic flux balance between upper and lower X-point in otherwise identical discharges [7].

Fig. 6(a) and (c), which may be due to HFS divertor detachment.

3.4. Edge plasma rotation

Toroidal plasma momentum is exchanged between the SOL and the edge at the separatrix due to diffusion, convection and viscosity. On the other hand, the SOL flow is mainly governed by the parallel pressure balance and classical drifts. The relationship between the edge rotation and SOL flow was investigated in the different divertor geometries of C-MOD [20]. The toroidal component of the SOL flow velocity (V_ϕ^{SOL}) near the separatrix, and the core toroidal rotation velocity (V_ϕ^{core}) are compared in Fig. 10 as a function of distance between primary and secondary separatrixes. In–out asymmetry in $M_\parallel$ profile is shown in Fig. 6, and, in particular, for USN, large negative value of $M_\parallel$ near the separatrix on the HFS midplane was pointed out: $V_\phi^{SOL\text{-}LFS} = -2$ km/s and $V_\phi^{SOL\text{-}HFS} = -40$km/s for USN, while $V_\phi^{SOL\text{-}LFS}$ and $V_\phi^{SOL\text{-}HFS} = 10$km/s for LSN. V_ϕ^{core} corresponds to -10 to -20 km/s for LSN and -30 to -40 km/s for USN. Decrements in $V_\phi^{SOL\text{-}LFS}$, $V_\phi^{SOL\text{-}HFS}$, V_ϕ^{core} from LSN to USN correspond to 50, 12, 16 km/s, respectively. It should be noted that $\Delta V_\phi^{SOL\text{-}HFS}$ is larger than ΔV_ϕ^{core}. This result suggests that the SOL flow affects the core rotation maybe through outward major radius convection from HFS SOL to the edge or through viscosity. Extending the investigation of the *coupling* between the edge and SOL plasmas at lower density (collisionality) or in H-mode will be important to understand not only the SOL flow but also edge rotation physics in the plasma boundary.

4. SOL flow simulation and driving mechanism

Drift effects have been implemented into 2D edge transport codes with realistic magnetic geometries (UEDGE [22,23], EDGE2D/Nimbus [24,19,5], B2SOLPS5.0 [25–28]), and many simulations lead to similar SOL flow patterns in qualitative agreement with those observed. Fig. 11 shows EDGE2D results as a function of the poloidal distance from the HFS divertor (L_p) in JET L-mode plasmas for the normal and reversed B_t [19]. The values of $D_\perp$ and $\chi_\perp$ are constant on the flux surfaces but their

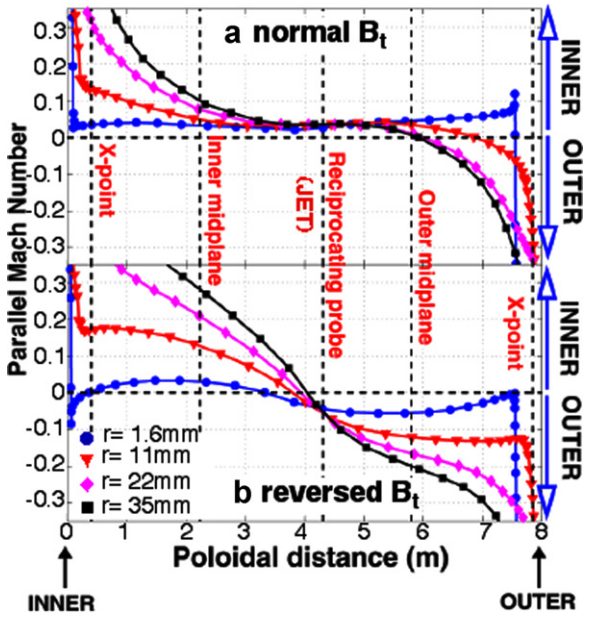

Fig. 11. EDGE2D simulation results including drifts, showing Mach numbers in JET as a function of the poloidal distance at four radial positions in the SOL (a) for forward B_t and (b) for reversed B_t [19].

radial profiles are varied to match the divertor plasma profiles. For the normal B_t, a stagnation point appears near the LFS midplane, and the SOL flow towards HFS divertor exists mostly in the main SOL ($L_p < 6$ m), whereas the stagnation point is near the plasma top ($L_p \sim 4$ m) for reversed B_t. For the normal B_t, the SOL flow directions from LFS midplane to HFS divertor (near the separatrix) is consistent with the measured SOL flow as shown in Fig. 1(b), and the shift of the stagnation point is reproduced with reversing B_t. However, the calculated flow is smaller than measured in the main SOL: EDGE2D does not account for the order of magnitude of the measurements, i.e. $M_{\|} = 0.3$–0.4 near the LFS midplane, $M_{\|} \sim 0.5$ near the plasma top, and $M_{\|} > 0.5$ at the HFS SOL. Most simulations also have difficulty in generating fast SOL flows in the far SOL. This piece of physics must be improved to simulate neutral and impurity recycling at the first wall [23]. Note that only the B2SOLPS5.0 calculation for C-MOD [27] achieved the experimentally observed values, namely $M_{\|} = 0.3$ at LFS midplane. The paper reported that the modelling of the electric field inside and outside the separatrix may influence the calculation of $M_{\|}$.

Modelling of the driving mechanisms for the fast SOL flow is currently an active area of research, with several avenues being explored. These include (i) torque generation due to difference in surface averaged $\langle j_r \rangle$ [21], (ii) coupling between turbulence and SOL flow via the Reynold's stress [29], (iii) global circulation due to outward movement of the edge plasma such as cross-field convection towards the HFS or LHS depending on the $\mathbf{B} \times \nabla B$ drift direction [30], or enhanced diffusion at the LFS edge (such as $D_{\perp} \sim 1/\mathrm{B}$ and more) [30–32].

In particular, models including drifts and in–out asymmetries in diffusion and/or convection coefficients have been tested in one or more 2D simulation codes (EDGE2D, B2SOLPS5.0, UEDGE) for different tokamak geometries in order to understand the effects on the SOL flow. The fast SOL flow such as $M_{\|} \sim 0.3$ at the LFS midplane (B2SOLPS5.0, UEDGE in C-MOD) and at the plasma top (EDGE2D, B2SOLPS in JET), and sonic-level at the HFS (UEDGE in C-MOD) was obtained using models (ii) and (iii) described above. Identification of the physics process of the in–out asymmetric radial transport such as blob, and systematic comparison with multi-machine experiments will be crucial for improving simulations.

5. SOL flow influence on impurity plume and transport

5.1. Impurity plume and influence on impurity

Problems with Mach probe interpretation, e.g. the influence of impurity cooling on the $M_{\|}$ magnitude [5] or difficulty in distinguishing between the parallel and toroidal components of the SOL flow [33], were pointed out. Recently, 2D image measurements of impurity plume (such as carbon and boron) have been developed at important poloidal locations such as the HFS midplane and above the LFS baffle in C-MOD [34,35], and at the plasma top in DIII-D [36,37]. The measurement can be applied when the collision time between bulk ion and impurity ion is shorter than the ionization time of the impurity. Here, parallel transport of impurity ions is determined by friction and thermal forces due to the bulk ions, which are described by the simple forms: $F_{\mathrm{fric}} \sim 1.6 \times 10^3 Z^2 n_i M_{\|} T_i^{-1}$[eV m^{-1}, 10^{19} m^{-3}, eV] (Z is impurity charge state), and $F_{i\text{-therm}} = 2.2 Z^2 \nabla_{\|} T_i$ [eV m^{-1}, eV], respectively [38].

Fig. 12 shows 2-D measurement of the C^{1+} line at HFS midplane for the LSN and USN divertors in C-MOD ohmic L-mode plasma [34]. Significant influence of the fast SOL flow on impurity plume

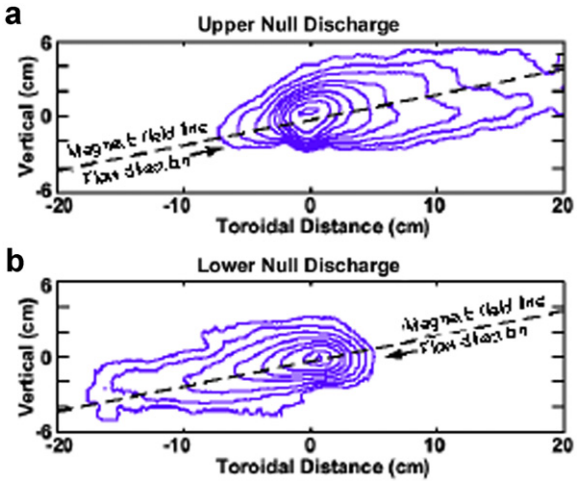

Fig. 12. Contour plots of C^{+1} dispersal (515 nm light, viewed along the major radius direction) resulting from CH_4 injection at the inner wall, midplane locations in C-MOD [34]. These data show strong plasma flow directed primarily along the field lines in the HFS SOL, with a clear dependence on LSN/USN topology.

is observed: a tail of the emission distribution is observed and is aligned towards the divertor along the field line both for LSN and USN. An ionization model with $M_{\|} \sim 0.4$ for the bulk ion is consistent with the emission image of C^{1+}. The fast bulk plasma flow is consistent with the Mach probe measurements. More localized measurement was performed above the LFS baffle in C-MOD using impurity puff from the inserted probe head [35]: while the direction was the same (away from the LFS divertor), the plume result ($M_{\|} = 0.18$) was smaller than the Mach probe measurement ($M_{\|} = 0.48$) at the separatrix (but $M_{\|}$ decreased at far SOL). In the case of large induced local E_r of the probe pre-sheath and/or short connection length in the downstream of the Mach probe, simple evaluation form of the Mach probe model [13] is not applicable. Fig. 13 shows impurity plumes of CII and CIII in DIII-D L-mode plasma by methane gas puff ($^{13}CH_4$) from the plasma top: carbon ions with higher charge states shifted further towards the HFS SOL. Monte-Carlo modelling (OEDGE: OSM+EIRINE+DIVIMP Edge) [39] demonstrated that subsonic SOL flow of $M_{\|} \sim 0.4$ with $D_{\perp} \sim 0.3\ m^2/s$ reproduced the poloidal shift of the emission regions towards the HFS SOL [36].

As a result, both impurity plume experiment and Mach probe measurement show that subsonic level of SOL flow towards the HFS divertor exists at the plasma top and the HFS SOL in ohmic and L-mode. Whereas the plume results above the LFS baffle showed relatively slow B_t-dependent SOL flow, quantitative comparison might be more reliable at the LFS midplane, where subsonic $\Delta M_{\|}$ (0.3–0.4) was observed in many Mach probe measurements.

5.2. Influence on impurity transport

Fast SOL flow towards the HFS divertor plays an important role in the carbon transport and

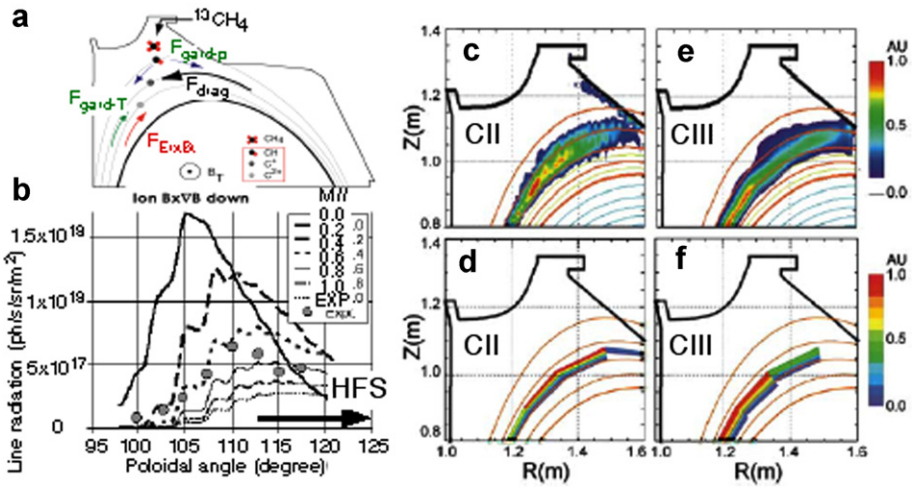

Fig. 13. (a) Plasma shape in DIII-D and gas puff from upper divertor. (b) Comparison of poloidal profile of CIII measured by the upward-looking Filter scope (absolutely calibrated) compared with code results based on various parallel Mach numbers, and $D_{\perp} = 0.3\ m^2/s$. Reconstructed 2D pictures from the toroidal viewing camera, in (c) CII and (d) CIII. Corresponding code results of (e) CII and (f) CIII, for $M_{\|} = 0.4$ and $D_{\perp} = 0.3\ m^2/s$. Same color bars for experiment and code. The camera pictures are occluded below $Z \sim 0.8$ m. [36]. (For interpretation of the references to colour this figure legend, the reader is referred to the web version of this article.)

deposition through the large friction force [1]. Understanding the effect of the fast SOL flow on carbon impurity has recently progressed.

First, the fast SOL flow is of direct relevance to particle control with divertor pumping and impurity screening. Previous measurements showed that neither ion flux nor $M_{\|}$ was increased during gas puffing into the main chamber during the divertor pumping, i.e 'puff and pump' (PP), in AUG [40] and JT-60U [41] although the impurity concentration in the main plasma was reduced. Measurements of the SOL flow at the HFS (above baffle) and LFS (midplane and X-point) SOLs during intense gas puffing at the plasma top ($1–3\times10^{22}\,s^{-1}$) were recently performed in JT-60U L-mode with the normal B_t [42], where only the HFS divertor plasma was partly detached. Only in the HFS SOL, both $M_{\|}$ and n_i (assuming $n_i = n_e$) in parallel component of ion flux density ($\gamma_{\|}^{HFS} = n_i M_{\|} C_s$) were 20–50% larger than those for the divertor gas puff (DP) at the same $\bar{n}_e$. The total ion flux towards the HFS divertor ($\Gamma_{\|}^{HFS}$) for PP was evaluated to be 1.4–1.7 times larger than $\Gamma_{\|}^{HFS}$ for DP, and the enhancement of F_{fric} was by a factor of 2–3 compared to $F_{i-therm}$. This fact was consistent with the reduction in the impurity concentration in the main plasma ($n_C/n_e = 0.8\%$ for PP and 1.2% for DP).

Second, the methane gas puff ($^{13}CH_4$) experiment in the DIII-D L-mode demonstrated the influence of the fast SOL flow on carbon deposition: ^{13}C deposition was dominant at the HFS divertor. OEDGE modelling of the carbon transport and deposition [43] showed that subsonic SOL flow with $M_{\|} = 0.3–0.6$ is essential to ^{13}C deposition on the HFS divertor, and that the deposition profile can be reproduced with medium convection of $D_{\perp} \sim 0.3–0.5\,m^2/s$. Recent methane gas puff study in ELMy H-mode with partially detached divertor as well as modelling [44] also showed that a SOL flow with $M_{\|} = 0.3–0.4$ is necessary for HFS deposition while $D_{\perp}$ hanged and a transport model for the ELM phase was introduced to reproduce the ^{13}C deposition profile.

SOL flow generated by $E_r \times B$ drift in the divertor private region was shown to be important in L-mode plasmas of DIII-D [45,46] and JT-60U [42]. This B_t-dependent transport plays an important role in producing the *HFS- and LFS-enhanced* asymmetry of the divertor plasma [45,42] as well as impurity recycling [23] for both *normal* and *reversed* B_t *cases*, respectively. This drift effect should be investigated in the divertor study.

6. Conclusions

Understanding SOL parallel plasma flow has progressed with development of diagnostics such as Mach probes and impurity plume to measure the SOL flow pattern at several poloidal locations. From experiments mainly from L-mode plasmas in many divertor tokamaks, the radial profile of the SOL parallel flow changes with poloidal location in the SOL due to a combination of two driving mechanisms, i.e. (1) classical drifts in the flux surfaces (B_t-dependent component) and (2) in–out asymmetry in radial diffusion/transport (basically B_t-independent component). In particular, the latter generates subsonic to sonic-level of fast SOL flow towards the HFS divertor, at least, in the HFS SOL (midplane and above baffle). The former enhances the fast SOL flow at the plasma top and LFS SOL for the ion $\mathbf{B}\times\nabla B$ drift downward and low density case. Quantitative determinations of drifts in the SOL, and understanding the influence of cross-field diffusion on parallel transport are crucial for improving model of SOL and divertor plasmas.

Important observations of SOL flow enhancement towards the HFS divertor such as (3) HFS divertor detachment and (4) intense gas puffing and divertor pumping, and (5) effect on the edge rotation, were recently obtained in L-mode plasmas. The fast SOL flow plays an essential role on impurity shielding from the main plasma and deposition profile on the HFS divertor, and it will influence the performance on core plasma (such as impurity shielding and L–H transition). All processes (1–5) will exist in a reactor, quantitative determination of their effects under various plasma conditions such as ELMy H-mode and detached divertor, as well as its modelling/simulation are crucial for divertor design and operation.

Acknowledgements

The author would like to thank members the ITPA SOL and divertor physics topical group, particularly, R.A. Pitts (*CRPP*), W. Fundamenski, K. Erents, (*EFDA-JET*), B. LaBombard, B. Lipschultz (*MIT*), M. Fenstermacher, M. Groth (*GA*), D. Elder, P. Stangeby (*Univ. Toronto*), A. Kallenbach, A. Chankin, D. Coster, M. Tsalas (*IPP*), X. Bonnin (*Univ. Paris*), G. Kirnev (*Kurchatov Inst.*) for support and contributions for this research. The author

would like to thank the JT-60 team (*JAEA*) for supporting experiments.

References

[1] G.F. Matthews, J. Nucl. Mater. 337–339 (2005) 1.
[2] N. Asakura, S. Sakurai, N. Hosogane, et al., Nucl. Fusion 39 (1999) 1983.
[3] N. Asakura, H. Takenaga, S. Sakurai, et al., Plasma Phys. Control. Fusion 44 (2002) 2101.
[4] S.K. Erents, A.V. Chankin, G.F. Matthews, P.C. Stangeby, Plasma Phys. Control. Fusion 42 (2000) 905.
[5] S.K. Erents, R.A. Pitts, W. Fundamenski, et al., Plasma Phys. Control. Fusion 46 (2004) 1757.
[6] B. LaBombard, J.A. Goetz, I.H. Hutchinson, et al., J. Nucl. Mater. 241–243 (1997) 149.
[7] B. LaBombard, J.E. Rice, A.E. Hubbard, et al., Nucl. Fusion 44 (2004) 1047.
[8] R. Pitts, et al., J. Nucl. Mater., these Proceedings, doi:10.1016/j.jnucmat.2006.12.065.
[9] J.A. Boedo, R. Lehmer, R.A. Moyer, et al., J. Nucl. Mater. 266–269 (1999) 783.
[10] M. Talsa et al., J. Nucl. Mater., these Proceedings.
[11] H.W. Muller et al., J. Nucl. Mater., these Proceedings, doi:10.1016/j.jnucmat.2006.12.054.
[12] J.P. Gunn et al., J. Nucl. Mater., these Proceedings, doi:10.1016/j.jnucmat.2007.01.195.
[13] I.H. Hutchinson, Phys. Rev. A 37 (1988) 4358.
[14] N. Asakura, S. Sakurai, O. Naito, et al., Plasma Phys. Control. Fusion 44 (2002) A313.
[15] W. Fundamenski et al., J. Nucl. Mater. 337–339 (2005).
[16] P.C. Stangeby, A.V. Chankin, Nucl. Fusion 36 (1996) 839.
[17] A.V. Chankin, P.C. Stangeby, Plasma Phys. Control. Fusion 38 (1996) 1879.
[18] N. Asakura, S. Sakurai, et al., Phys. Rev. Lett. 84 (2000) 3093.
[19] R. Pitts, P. Andrew, X. Bonnin, et al., J. Nucl. Mater. 337–339 (2005) 146.
[20] B. LaBombard, J.E. Rice, A.E. Hubbard, et al., Phys. Plasmas 12 (2005) 056111.
[21] A.V. Chankin, P.C. Stangeby, Nucl. Fusion 41 (2001) 421.
[22] G.D. Porter, R. Isler, J. Boedo, Phys. Plasmas 7 (2000) 3663.
[23] G.D. Porter, T.D. Rognlien, M.E. Rensink, et al., J. Nucl. Mater. 313–316 (2003) 1085.
[24] A.V. Chankin, G. Corrigan, S.K. Erents, et al., J. Nucl. Mater. 290–293 (2001) 518.
[25] R. Schneider, D. Coster, B. Braams, et al., Contrib. Plasma Phys. 40 (2000) 328.
[26] V.A. Rozhansky, S.P. Voskoboynikov, E.G. Kaveeva, et al., Nucl. Fusion 41 (2001) 387.
[27] X. Bonnin, D. Coster, R. Schneider, et al., J. Nucl. Mater. 337–339 (2005) 301.
[28] X. Bonnin et al., 32nd EPS, 2005, p. P-2.110.
[29] C. Hidalgo, B. Gonçalves, M.A. Pedrosa, et al., J. Nucl. Mater. 313–316 (2003) 863.
[30] G.S. Kirnev, G. Corrigan, D. Coster, et al., J. Nucl. Mater. 337–339 (2005) 271.
[31] T.D. Rognlien, M.V. Umansky, X.Q. Xu, et al., J. Nucl. Mater. 337–339 (2005) 327.
[32] A.Yu. Pigarov, S.I. Krasheninnikov, B. LaBombard, 10th International Workshop on plasma Edge Theory in Fusion Devices, 17–19 October 2005, Julich.
[33] B. LaBombard, S. Ganagadhara, B. Lipschultz, et al., J. Nucl. Mater. 313–316 (2003) 995.
[34] D. Jablonski, B. LaBombard, G.M. McCracken, et al., J. Nucl. Mater. 241–243 (1997) 782.
[35] S. Ganagadhara, B. LaBombard, Plasma Phys. Control. Fusion 46 (2004) 1617.
[36] A.G. McLean, J.D. Elder, P.C. Stangeby, et al., J. Nucl. Mater. 337–339 (2005) 124.
[37] M. Groth, L.W. Owen, G.D. Porter, et al., J. Nucl. Mater. 337–339 (2005) 425.
[38] J. Neuhauser et al., Nucl. Fusion 24 (1984) 39.
[39] P.C. Stangeby, J.D. Elder, J.A. Boedo, et al., J. Nucl. Mater. 313–316 (2003) 883.
[40] H.-S. Bosch, R. Dux, G. Haas, et al., Phys. Rev. Lett. 76 (1996) 2499.
[41] N. Asakura, S. Sakurai, H. Tamai, et al., J. Nucl. Mater. 290–293 (2001) 825.
[42] N. Asakura, H. Takenaga, S. Sakurai, et al., Nucl. Fusion 44 (2004) 503.
[43] J.D. Elder, P.C. Stangeby, D. Whyte, et al., J. Nucl. Mater. 337–339 (2005) 79.
[44] J.D. Elder, A.G. McLean, P.C. Stangeby, et al., these Proceedings (P1-9).
[45] J.A. Boedo, M.J. Schaffer, R. Maingi, et al., Phys. Plasmas 7 (2000) 1075.
[46] M.J. Schaffer, J.A. Boedo, R.A. Moyer, et al., J. Nucl. Mater. 290–293 (2001) 530.